Available online at www.sciencedirect.com
SCIENCE DIRECT®
Journal of Nuclear Materials 350 (2006) 301–309
journal of nuclear materials
www.elsevier.com/locate/jnucmat

# Thermal properties of redeposition layers in the JT-60U divertor region

Y. Ishimoto *, Y. Gotoh, T. Arai, K. Masaki, N. Miya, N. Oyama, N. Asakura

*Fusion Research and Development Directorate, Japan Atomic Energy Agency, Mukoyama 801-1, Naka, Ibaraki 311-0193, Japan*

Received 21 June 2005; accepted 21 January 2006

**Abstract**

Thermal properties of the redeposition layer on the inner plate of the W-shaped divertor of JT-60U have been measured with laser flash method so as to estimate transient heat loads onto the divertor. Morphology analysis of the redeposition layer was conducted with a scanning electron microscope. Measurement of a redeposition layer sample of more than 200 μm thick, which had been produced near the most frequent striking point, showed following results: (1) the bulk density of the redeposition layer is about half of that of carbon fiber composite material; (2) the specific heat of the layer is roughly equal to that of the isotropic graphite; (3) the thermal conductivity of the redeposition layer is two orders of magnitude smaller than that of the carbon fiber composite. This low thermal conductivity of the redeposition layer is considered to be caused by a low graphitization degree of the redeposition layer. The difference between the divertor heat loads and the loss of the plasma stored energy becomes smaller taking account of thermal properties of the redeposition layer on the inner divertor, whereas estimated heat loads due to the ELMs is still larger than the loss. This is probably caused by the poloidal distribution of the thermal properties.
© 2006 Elsevier B.V. All rights reserved.

*PACS:* 52.40.Hf

## 1. Introduction

It is widely recognized that the evaluation of both erosion due to physical or chemical sputtering and redeposition is an important issue in designs of the fusion reactor using carbon based plasma-facing materials [1,2]. In particular, divertor tiles are considered to be eroded severely due to not only steady heat loads but also transient ones such as Edge Localized Modes (ELMs) in ITER. The evaluation of transient heat loads is essential for the lifetime assessment of the divertor tiles. Thermal properties of the surface are necessary to estimate transient heat loads with an infrared (IR) camera of high time-resolution. However a database of thermal properties of the redeposition layer has been insufficient. Therefore thermal properties of the layer formed in actual devices have been required to estimate transient heat loads onto the divertor tiles.

ELMs which produce a periodic loss of particles and energy from edge plasma are often observed in H-mode discharges [3]. Among a variety of ELMs,

* Corresponding author. Tel.: +81 292707437; fax: +81 292707449.
*E-mail address:* ishimoto.yuki@jaea.go.jp (Y. Ishimoto).

0022-3115/$ - see front matter © 2006 Elsevier B.V. All rights reserved.
doi:10.1016/j.jnucmat.2006.01.013

Type-I ELMs largely increase sputtering of first wall materials. The characteristic pulse length of Type-I ELMs is 250–500 μs on the divertor targets and the maximum heat flux exceeds 100 MW/m$^2$ in the case of JT-60U [4]. Transient heat loads to target tiles due to ELMs are calculated from time evolution of the surface temperature measured with an IR-camera [5], therefore thermal properties of the surface are essential for this estimation. However the thermal property of the redeposition layer is considered to be different from that of the tile material as shown in the recent reports: the surface temperature of the redeposition layer on the TFTR carbon tiles was found to be larger than that of the bare tile, where the tiles are irradiated with the same power of a scanning laser in detritiation experiments [6]; the redeposition layer formed on the tile surface is treated as heat resistance in thermal analyses in other tokamaks [7–9].

In JT-60U, it has been found that redeposition and erosion is dominant in the inner and the outer divertor tiles, respectively [10], and the heat loads caused by ELMs to divertor tiles estimated from the IR-camera are 2–5 times larger than the loss of the plasma stored energy [11]. The heat loads to the divertor must be smaller than loss of the stored energy because the source of the heat loads is considered to be the particle and energy lost from the core plasma during ELMs. Considering columnar porous structure in the redeposition layer observed in JT-60U [12], the thermal conductivity of the layer is expected to be much smaller compared with that of the tile substrate. Thus, if it is true, the heat load to the inner target tiles is overestimated. Since the heat flux does not reach the interface between the redeposition layer and the substrate during the duration time of a single ELM, the surface temperature depends on only the thermal properties of the layer. Therefore it is necessary to measure thermal properties of the redeposition layer in order to estimate transient heat loads caused by ELMs. This paper describes thermal properties of the redeposition layer formed on the inner divertor tile used in deuterium discharge experiments in JT-60U.

## 2. Experimental procedure

### 2.1. Sample tiles

JT-60U has been operated with the W-shaped divertor since 1997. The cross-sectional schematic of the W-shaped divertor is shown in Fig. 1(b). Inside of the Inconel vacuum vessel is fully covered with carbon tiles. Isotropic graphite has been used for first walls and inner dome wing tiles. Carbon fiber composite (CFC) materials are used for the baffle and the divertor regions to tolerate high heat and particle loads. The divertor tiles used as specimens were exposed to about 10 600 deuterium and 1500 hydrogen plasma discharges from 1997 to 2002 and were extracted from the vacuum vessel in 2003. The exposure duration of these tiles to divertor plasmas is about 90 000 s. The maximum neutral beam injection power was ~25 MW. Although, in usual operation, hydrogen plasma discharges are conducted before ventilation in order to degas tritium generated by DD reaction, they were not carried out before the ventilation in 2003.

The tiles were removed in the air atmosphere and stored in vacuum-packs until they were cut into the sample pieces. The redeposition layer of more than 200 μm thick was selected as the samples. A thin sample makes the laser flash measurement difficult as mentioned in Section 2.3.1. There is also technical reason that a thin sample is easily broken during the treatment of the sample. Samples ($\phi 6 \times 0.6$ mm)

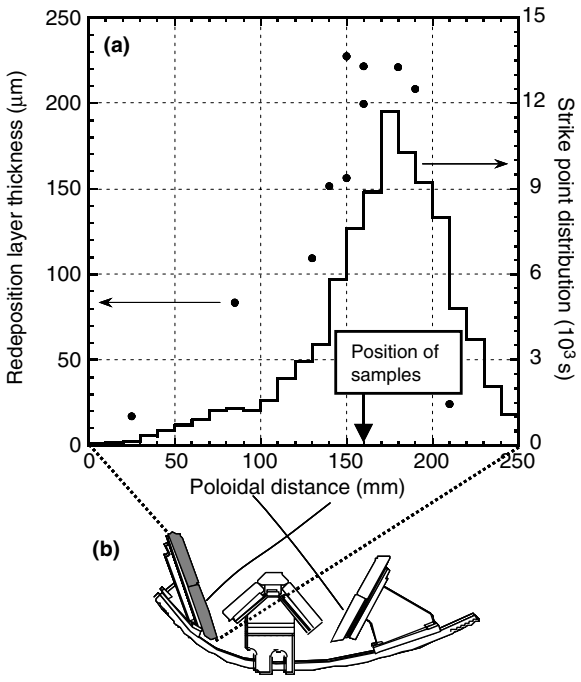


Fig. 1. (a) Poloidal profiles of the redeposition layer thickness on the inner tile surface and the distribution of the inner striking point and (b) cross-sectional view of the W-shaped divertor. The origin of the horizontal axis corresponds to the inner edge of the target tile (shaded area).

were cut from the inner divertor target plate using a diamond cutter and a file. In order that the samples consist of only redeposition layer, the tile substrate (CFC) of the samples was carefully removed by means of fine sandpaper until the thickness of the sample measured with a dial gauge is equal to the redeposition layer thick observed by SEM (Scanning Electron Microscopy).

### 2.2. SEM analyses

SEM (S-3000H, Hitachi) was used to observe the morphology of the redeposition layer and to measure its thickness. The observed surface was perpendicular to the plasma-facing side and was prepared by mechanically fracturing along the slit that is formed from the rear surface. The acceleration voltage was set to be 4.91 kV for the surface structure observation because the sample mainly consists of light elements (B, C and O).

### 2.3. Thermal property measurements

#### 2.3.1. Thermal diffusivity

Thermal diffusivity of the redeposition layer was measured with the laser flash method [13] (LFA427, NETZSCH). As shown in Fig. 2, a sample was irradiated with a short pulsed laser and the backside temperature was monitored with an IR detector (liquid–nitrogen–cooled InSb). One-dimensional heat transfer problem in the diagram can be solved analytically assuming that the sample is adiabatic. Based on the Parker's expression [13], the thermal diffusivity $\alpha$ of the sample is determined from the sample thickness $l$ and half rise time $t_{1/2}$ at which the backside temperature reaches the half of the maximum

$$\alpha = \frac{0.1388 l^2}{t_{1/2}}. \quad (1)$$

The influence of heat loss from the sample on the thermal diffusivity was estimated from the Cowan's model [14]. Although the pulse length of the laser was set to be 0.3 ms for short $t_{1/2}$ ($\sim$ several ms), the finite pulse length correction was also applied. An attenuation filter was installed between the laser unit and the sample to avoid overheating of the sample because the weight of the sample was of the order of milligram. Absorbed energy was estimated to be about 1 mJ. Measurements were conducted five times at every additional 100 °C as the sample temperature was raised from room temperature (RT) up to 1000 °C. Heating rates of 5–20 °C/min were employed so as to stabilize the sample temperature. The vacuum vessel of LFA427 is pumped out by the turbo molecular pump and the pressure is sustained below $10^{-2}$ Pa during the measurement. Temporal evolution of a typical detector signal and a laser pulse shape are shown in Fig. 3.

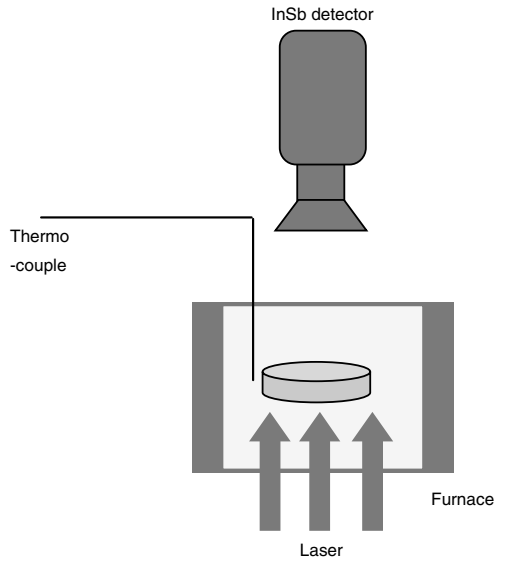


Fig. 2. Schematic diagram of the laser flash method.

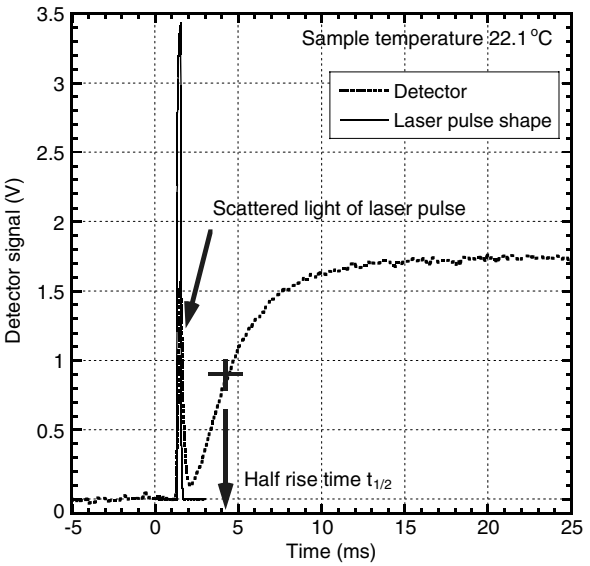


Fig. 3. Time evolution of the detector signal and the laser pulse shape. The simultaneous peak of the detector signal is due to scattered laser.

The peak of the detector signal, which is simultaneous with the laser flash, is due to scattered laser. A thin sample makes the laser flash measurement difficult because half rise time is proportional to the square of the sample thickness. In order to obtain sufficient accuracy, half rise time of more than ~2 ms is required from the result of our verification experiment.

#### 2.3.2. Specific heat

The specific heat of the redeposition layer was measured by comparing with a reference. In order to avoid the influence of the chemical change due to heat up, the sample for the specific heat measurement was newly cut out from the position adjacent to the sample used for the thermal diffusivity measurement. The sample and the reference material (isotropic graphite, ETP-10) were coated with graphite spray so that the emissivity and the adsorption coefficient of both samples were on equal terms. Mass of the sample was weighed on the microbalance before and after graphite coating for the sake of correcting mass increase due to graphite coating. Thickness of graphite coating was measured to be about 5 μm with SEM. The increment of the detector signal caused by laser irradiation was measured. The specific heat at constant pressure of the sample $C_p$ is obtained from the following equation:

$$C_p = \frac{\Delta V_{\mathrm{ref}}}{\Delta V}\frac{Q}{Q_{\mathrm{ref}}}\frac{m_{\mathrm{ref}}}{m}C_{p\,\mathrm{ref}}, \tag{2}$$

where the subscript 'ref' denotes the reference, m is mass of the sample, $\Delta V$ is the increment of the detector signal and $Q$ is adsorbed energy due to laser irradiation, respectively. Temporal evolution of the sample temperature is fitted to the exponential function, and $\Delta V$ immediately after laser irradiation is determined by extrapolating the function to $t = 0$. The specific heat of isotropic graphite tabulated in Ref. [15] was used as $C_{p\,\mathrm{ref}}$. $Q$ was estimated from the time integral of the pulse shape function measured shot by shot with a diode detector.

#### 2.3.3. Bulk density

Bulk density of the redeposition layer is indispensable to calculate the thermal conductivity of the redeposition layer. To estimate this value, the thickness of the sample was measured with a dial gauge (resolution: ~3 μm), and the area of the sample was estimated by counting pixels in the photograph of the sample because the sample edge is chipped during cutting. The mass of the sample was weighed on a microbalance.

## 3. Results and discussion

### 3.1. Results

Fig. 1(a) shows the poloidal profiles of the redeposition layer thickness and the distribution of the striking point on the inner tile surface. The maximum thickness of the redeposition layer was found to be 220 μm near the most frequent striking point. Analyzed samples were extracted from this point because one of objectives in this study is to improve estimation of transient heat fluxes. Cross-sectional SEM images of the redeposition layer on the inner divertor tile of JT-60U are shown in Fig. 4. Fig. 4(a) shows that columnar structure is found on the tile substrate and the axes of columns are inclined. On the other hand, one can see in Fig. 4(b) that laminar structure parallel to the tile surface is developed. Although columnar structure is confirmed to be dominant in the sample from the SEM observation, laminar structure is partly observed under the columnar structure layers. It is difficult to obtain the sample which completely consists of columnar or laminar structure in an actual plasma device. Thus we treat the value of thermal diffusivity as an effective value in this study. Laminar and columnar structure was confirmed in the layer as stated in Ref. [10]. The detailed description of columnar and laminar structure formation was reported in Ref. [12].

The thickness and the area of the sample for the bulk density measurement were $1.5 \times 10^{-4}$ and $2.2 \times 10^{-5}$ m$^2$, respectively. The mass of the sample was $3.0 \times 10^{-3}$ g. Therefore the bulk density of the redeposition layer was 910 kg/m$^3$ at the inner striking point. This is about half of the density of tile substrate (1700 kg/m$^3$, CX-2002U). The result did not contradict the SEM observation which showed the porous structure of the redeposition layer.

Fig. 5 shows temperature dependence of the thermal diffusivity of the redeposition layer and other carbon materials (CFC, isotropic graphite, glassy carbon and pyrolytic graphite perpendicular to the basal plane). These materials were also measured with the same way to compare with the redeposition layer. It was found that the thermal diffusivity of the redeposition layer is about two orders of magnitude smaller than that of the tile substrate. Thermal diffusivity of the specimen cut from the erosion

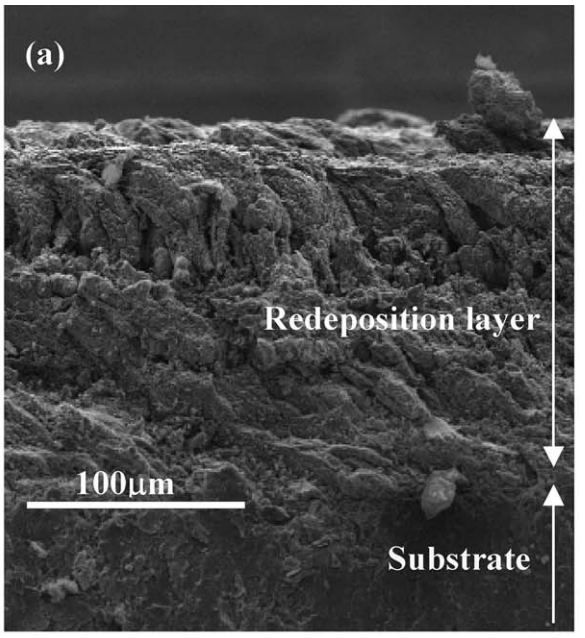


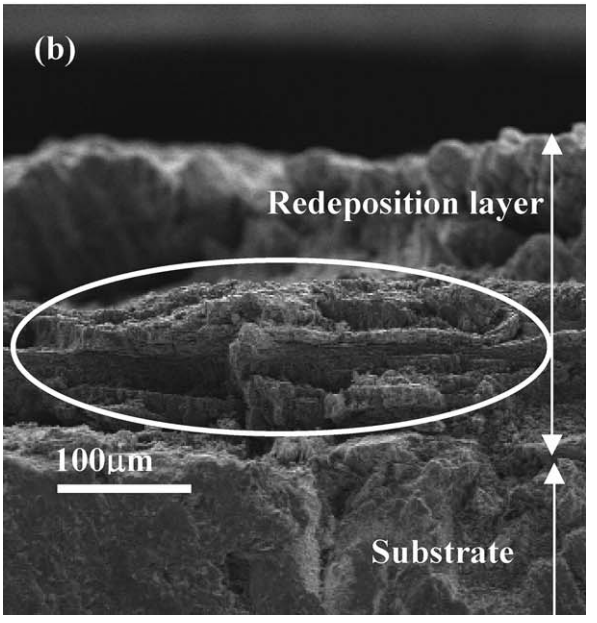


Fig. 4. Cross-sectional view of the redeposition layer. (a) Columnar structure and (b) laminar structure (inside of the oval). These samples were removed from the inner divertor plate, as shown in Fig. 1(a).

dominant region (i.e. the outer divertor target) was also measured and was found to be 15% smaller than that of the tile substrate at RT. However there is the maximum of the 10% difference in the thermal diffusivity of each production lot for CX-2002U. The difference of thermal diffusivity between the erosion region and the substrate does not have a great effect on estimation of ELMs heat loads on the outer divertor.

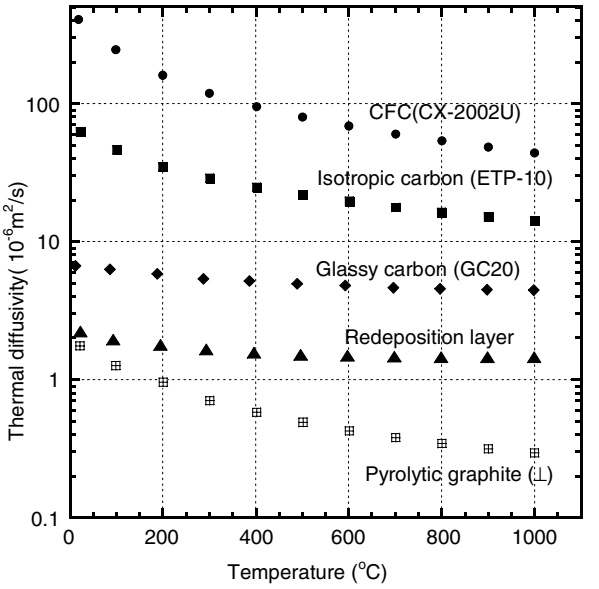


Fig. 5. Temperature dependence of the thermal diffusivity of the redeposition layer and other carbon materials (CFC, isotropic graphite, glassy carbon and pyrolytic graphite perpendicular to the basal plane).

Specific heat is necessary to estimate heat flux through the surface temperature rise. As shown in Fig. 6, it was found that the specific heat of the redeposition layer is almost equal to that of the reference at the temperature range from RT to 1000 °C within experimental error. This result is considered to be reasonable because the redeposition layer is mainly made up of carbon as a result of X-ray photoelectron spectroscopy [10].

### 3.2. Thermal conductivity

Temperature dependence of thermal conductivity $k$ calculated by means of the equation $k = \alpha\rho C_p$ is shown in Fig. 7. It was confirmed that $k$ of the redeposition layer is two orders of magnitude smaller than that of the tile substrate. While $k$ of both the layer and glassy carbon increased with temperature, others had the opposite temperature dependence. The temperature dependence of $k$ of the former reflects those of the specific heat due to the smaller drop of the thermal diffusivity with increasing temperature.

Heat transfer in graphite materials is explained by the phonon conduction theory. Since the group velocity of phonons parallel to the basal plane is

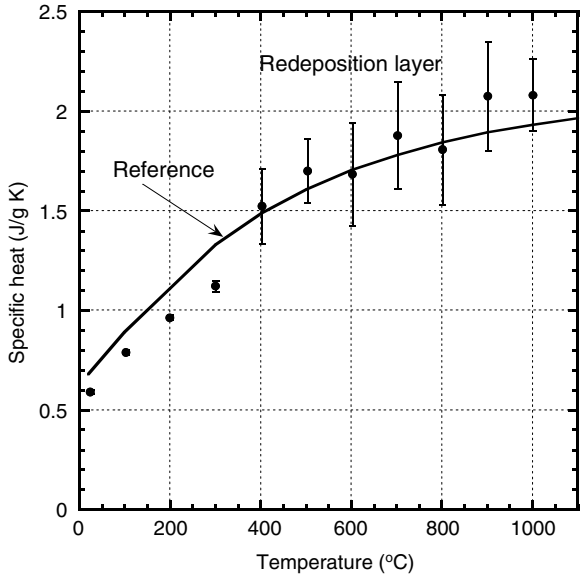


Fig. 6. Temperature dependence of the specific heat of redeposition layer. The solid line shows the value of the reference (isotropic graphite, AXF-5Q) [15].

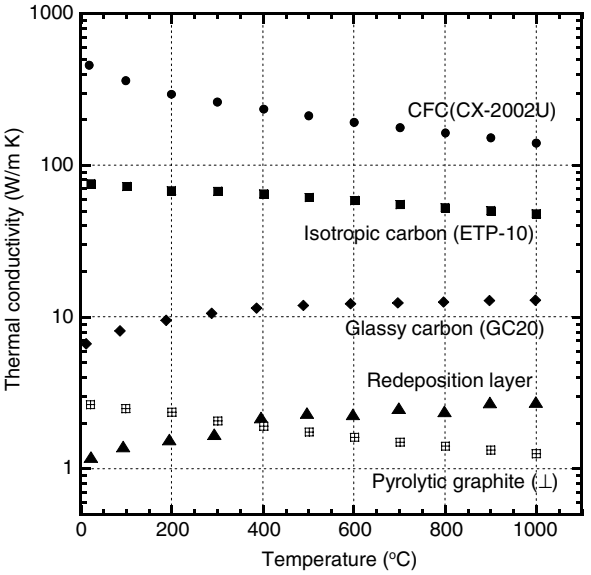


Fig. 7. Temperature dependence of the thermal conductivity of the redeposition layer and other carbon materials (CFC, isotropic graphite, glassy carbon and pyrolytic graphite perpendicular to the basal plane).

much larger than the velocity perpendicular to the basal plane, heat conduction perpendicular to the basal plane is negligible in polycrystalline graphite materials. Because the typical operation temperature range of inner divertor targets is from 573 K to 1273 K, it is considered that the layer has a lower degree of graphitization. Thus it is assumed that the redeposition layer can be treated as a polycrystalline material. The thermal conductivity depends on group velocity parallel to the basal plane $v$ and mean free path $l$ of phonons and the specific heat at constant volume $C$ [16,17]

$$k = \frac{1}{3}Cvl, \tag{3}$$

$$\frac{1}{l} = \frac{1}{l_g} + \frac{1}{l_U}, \tag{4}$$

where $l_g$ and $l_U$ are mean free path of phonons caused by the structure of the material and phonon–phonon scattering (Umklapp process), respectively. $l_g$ includes scattering at the grain boundaries and the structural influence of pores. It is assumed that the influence of impurity and phonon–electron scattering are negligible. Phonon–phonon scattering becomes dominant in a high temperature and mean free path caused by this process has $1/T$ dependence [16]. Thus we can rewrite Eq. (4) by using a constant $a$,

$$\frac{1}{l} = \frac{1}{l_g} + aT. \tag{5}$$

The equation $\alpha = k/C$ is used to remove the influence of the specific heat, and then the following equation is obtained:

$$\frac{1}{\alpha} = \frac{3}{v}\left(\frac{1}{l_g} + aT\right). \tag{6}$$

This equation indicates that a plot of $1/\alpha$ vs. $T$ results in a straight line when $v$ is assumed to be constant. The $y$-axis intercept is inversely proportional to $l_g$. Fig. 8 shows the inverse of thermal diffusivity as a function of temperature at a relatively high temperature range (>700 K). The data of CFC were not plotted in Fig. 8 due to small $y$-axis intercept of CFC and the experimental error. Because heat conduction of the pyrolytic graphite perpendicular to the deposition plane is caused by the phonon conduction perpendicular to the basal plane, the data of pyrolytic graphite perpendicular to the basal plane were also not plotted in the figure. The vertical axis is in an arbitrary unit because two constants ($a$ and $v$) are unknown. As shown in Fig. 9, it was confirmed that $l_g$ has a positive correlation with the thermal conductivity. The thermal conductivity at RT was used as a representative in this figure. Therefore it is suggested that the reason for extremely low thermal conductivity of the redeposition

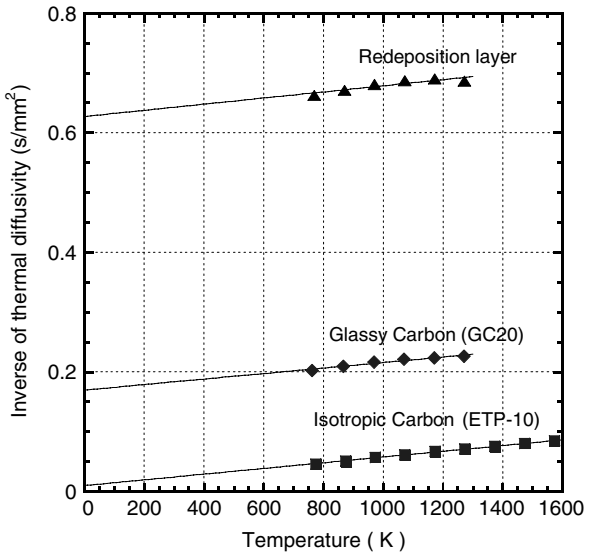


Fig. 8. Temperature dependence of the inverse of thermal diffusivity. Each $y$-axis intercept is inversely proportional to the mean free path due to their structure.

layer is smaller mean free path of phonons compared with other carbon material. This smaller mean free path seems to be due to low degree of graphitization because the surface temperature of divertor tiles was much lower than 1800 K at which some of carbon materials start graphitization. Although the graphitization degree of the redeposition layer on the JT-60U W-shaped divertor has not been measured yet, carbonaceous material of highly disordered lattice structure was found in the redeposition layer on lower-X-point divertor of JT-60 by using the selected area electron diffraction method [12]. It was also reported that the amorphous carbon matrix of the deposition layer on the limiter block of TEXTOR was observed by TEM techniques and this carbon matrix was characterized by staking of pseudo-two-dimensional graphitic planes parallel to the limiter [18]. These two results suggest low graphitization degree of the redeposition layer formed in JT-60U.

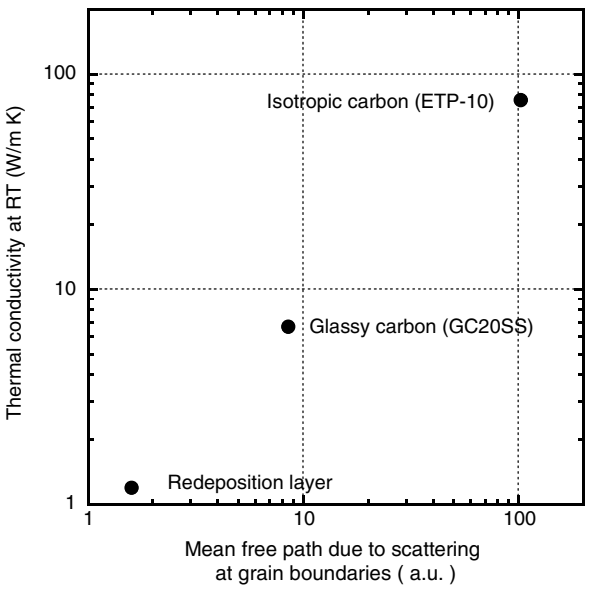


Fig. 9. Correlation between the mean free path of phonons due to the structure and thermal conductivities at RT. The thermal conductivity at RT is used as a representative in this figure.

### 3.3. Application to evaluation of heat loads

Transient heat loads due to Type-I ELMs is one of important issues in the ELM studies as mentioned above. The characteristic depth of heat transfer is estimated to be a few tens of μm within the pulse length of Type-I ELMs (250–500 μs) taking into account the thermal properties of the redeposition layer. Thus, since the heat transfer equation in the semi-infinite solid is applicable to estimate heat loads due to Type-I ELMs, the correlation between heat flux to the surface $q$ and increase of the surface temperature $\Delta T$ is expressed by the following equation:

$$q = \frac{\Delta T}{2}\sqrt{\frac{\pi k \rho C_p}{t}}, \tag{7}$$

where $t$ is the pulse length of the heat load. In the case of the same $\Delta T$, the ratio of $q$ is proportional to the ratio of $(k\rho C_p)^{1/2}$. Therefore the heat flux to the redeposition layer is one order of magnitude smaller than that to the tile substrate for the same $\Delta T$, because $k$ of the redeposition layer is two orders of magnitude smaller than that of the tile substrate.

Fig. 10 shows total divertor heat loads estimated from $\Delta T$ measured with the IR-camera as a function of the loss of the stored energy by ELMs. Data shown in Fig. 10 were obtained under following experimental conditions: the plasma current was 1.0–2.3 MA, the toroidal magnetic field was 1.9–4.0 T, the safety factor at 95% of the flux surface was 3.0–4.2 and $P_{NB}$ was 4.5–27.5 MW. The divertor heat load is estimated from time integral of a single ELM heat flux assuming that the heat flux is toroidally uniform. It was found through the above discussion that the heat flux to the redeposition

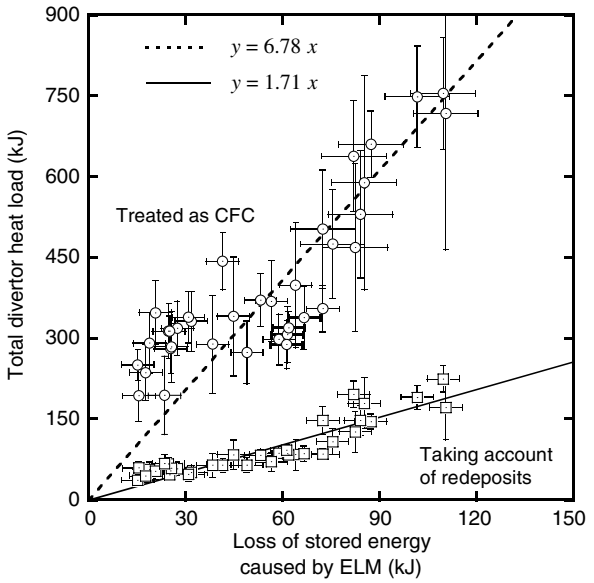


Fig. 10. Total divertor heat loads estimated from the IR-camera as a function of the loss of the stored energy by ELMs.

layer is 10% of that estimated using the thermal conductivity of the tile substrate. Thermal properties of the outer divertor are assumed to be equal to those of the tile substrate because thermal diffusivity of the specimen cut from the outer divertor tile is almost same as that of the tile substrate at RT. The total heat loads to the divertor tiles used to be estimated as 6.8 times larger than the loss of the stored energy. The difference between the divertor heat loads and the loss of the stored energy becomes smaller taking account of thermal properties of the redeposition layer on the inner divertor, whereas estimated heat loads due to the ELMs is still 1.7 times larger than the loss. This is probably caused by the poloidal distribution of the thermal properties. As shown in Fig. 1(a), the measured sample was cut from the position where the layer was more than 200 μm thick because of its fragileness. Although it is considered that the thermal properties of the layer depend on the tile temperature and plasma parameters, the thinner layer has not been measured due to accuracy of the data and difficulty of preparing samples. This is proposed as future work.

## 4. Conclusions

In order to estimate transient heat loads due to the ELMs more precisely, thermal properties of the reposition layer formed during the JT-60U deuterium experiments were measured with the laser flash method. Morphology analysis of the redeposition layer was also conducted with a SEM. Thicknesses of redeposition layers of more than 200 μm were observed at near the most frequent striking point. The bulk density of the redeposition layer was found to be 910 kg/m$^3$. It was shown that the specific heat of the redeposition layer is almost equal to that of isotropic graphite. The thermal conductivity of the redeposition layer was calculated to be two orders of magnitude smaller than that of the tile substrate in the temperature range from RT to 1000 °C. This low thermal conductivity of the redeposition layer is considered to be caused by a low graphitization degree of the redeposition layer. The difference between the divertor heat loads and the loss of the stored energy becomes smaller taking account of thermal properties of the redeposition layer on the inner divertor, whereas estimated heat loads due to the ELMs is still larger than the loss. This is probably caused by the poloidal distribution of the thermal properties. It is concluded that the lower thermal conductivity of the redeposition layer has a great influence on the estimation of transient heat loads such as ELMs.

## Acknowledgements

The authors would like to thank the JT-60U team for their support of sample preparation and analyses. They also acknowledge valuable discussions and helpful comments with Professor T. Tanabe of Kyushu University and Dr. M. Kuriyama of JAEA.

## References

[1] G. Federici et al., Nucl. Fus. 41 (2001) 1967.
[2] G. Federici et al., J. Nucl. Mater. 313–316 (2003) 11.
[3] D.N. Hill, J. Nucl. Mater. 241–243 (1997) 182.
[4] N. Asakura et al., Plasma Phys. Control. Fus. 44 (2002) A313.
[5] K. Itami et al., J. Nucl. Mater. 220–222 (1995) 203.
[6] C.H. Skinner et al., Phys. Scr. T103 (2003) 34.
[7] A. Herrmann, ASDEX Upgrade team, in: 28th EPS Conference on Controlled Fusion and Plasma Physics, ECA 25A, 2001, p. 2109.
[8] Y. Corre et al., in: 30th EPS Conference on Controlled Fusion and Plasma Physics, ECA 27A, 2003, p. 1.164.
[9] P. Andrew et al., J. Nucl. Mater. 313–316 (2003) 135.
[10] Y. Gotoh et al., J. Nucl. Mater. 313–316 (2003) 370.
[11] N. Asakura, in: 1st ITPA Meeting on SOL and Divertor Physics Topical Group, GA, 2002/2/25-27.

[12] Y. Gotoh et al., J. Nucl. Mater. 329–333 (2004) 840.
[13] W.J. Parker et al., J. Appl. Phys. 32 (1961) 1679.
[14] R.D. Cowan, J. Appl. Phys. 34 (1963) 926.
[15] R.E. Taylor, H. Groot, High Temp. High Press. 12 (1980) 147.
[16] C. Kittel, Introduction to Solid State Physics, 6th Ed., John Wiley, 1986.
[17] B.T. Kelly, in: P.L. Walker (Ed.), Chemistry and Physics of Carbon, vol. 5, p. 119.
[18] S. Muto et al., J. Nucl. Mater. 290–293 (2001) 295.